Journal of Microscopy, Vol. 209, Pt 3 March 2003, pp. 188–193
Received 10 August 2002; accepted 25 October 2002

Phase separation in polyfluorene – polymethylmethacrylate blends studied using UV near-field microscopy

J. CHAPPELL & D. G. LIDZEY
Department of Physics & Astronomy, The University of Sheffield, Hicks Building, Hounsfield Road, Sheffield S3 7RH, U.K.

Key words. Fluorescence, PFO, phase separation, polymer, NSOM, UV.

Summary

In this paper we present a near-field microscopy study of thin films of a phase-separated blend of the fluorescent conjugated-polymer poly(9,9-dioctylfluorene) [PFO] with the non-fluorescent polymer polymethylmethacrylate [PMMA]. A scanning near-field optical microscope (NSOM) was used to generate (blue) fluorescence from the PFO following UV excitation at 362 nm. A range of different concentrations of PFO in PMMA were studied ranging from 1 to 50% PFO in PMMA by mass. By studying both the shear force and fluorescence images we were able accurately to determine the distribution of PFO in the PMMA. We found that phase separation occurs over a number of different length-scales between 5 µm and 250 nm. We show that at PFO concentrations of 1%, the PFO lies on top of the PMMA. At a PFO relative concentration of 50%, the PMMA phase extends through the whole thickness of the film to the underlying substrate. We use such samples to discuss the resolution of NSOM when imaging thick organic films. Furthermore, we confirm that the length-scales of phase separation can be modified via control over spin-casting protocols.

Introduction

Scanning near-field optical microscopy (NSOM) (Paesler & Moyer, 1996), offers many advantages over conventional far-field optical microscopy as it can combine high-resolution topographic maps of a surface with optical information over length-scales significantly smaller than the wavelength of light. NSOM has been used by a number of authors to study the fluorescence emission from organic thin films, and in particular has been used to study the mechanisms of phase separation between different polymers (DeAro *et al.*, 1997; Hsu *et al.*, 1998; Webster *et al.*, 1998). Such systems are of great interest, as conjugated polymers are likely to find important applications in a range of different optoelectronic devices. There is clearly a need to gain a deeper understanding of the structure of disordered organic films, as the link between structure and function will be important in the optimization of device performance. Because of this, a number of studies have shown that fluorescence NSOM can be used to determine the composition of phase-separated thin polymer films (DeAro, 1997; Hsu, 1998; Webster, 1998; Stevenson *et al.*, 2001a; Stevenson *et al.*, 2001b), even those containing two or more fluorescent polymers in a common transparent matrix (Stevenson *et al.*, 1999). Furthermore, NSOM has been combined with fluorescence decay-lifetime measurements to study the relative importance of non-radiative channels in thin-films of conjugated polymers (Kwak *et al.*, 2001; Nabetani *et al.*, 2001). Other work has used near-field photoconductivity measurements to study the structure of stretched aligned conjugated-polymer films (DeAro & Buratto, 1999).

The polymer poly (9,9-dioctylfluorene) (PFO) has recently received particular attention in NSOM studies (Teetsov, 2000, 2002; Kwak *et al.*, 2001), as it is a state-of-the-art material used in organic light emitting diodes (OLEDs) (Grice *et al.*, 1998). PFO emits blue fluorescence with high quantum efficiency (in excess of 50% in a thin film; Virgili *et al.*, 2000), and is characterized by a high hole carrier mobility (Redecker *et al.*, 1999). Recent studies (Teetsov, 2000) have shown that thin films of PFO have a degree of long-range order and contain polarized domains of 50–500 nm in size. The same authors also demonstrated that pristine PFO films contain aggregated polymer clusters of diameter 50–150 nm that are less emissive. Furthermore, NSOM studies (Teetsov, 2002), have confirmed that annealed PFO films show high degrees of local organization (Grell *et al.*, 1999).

In this paper, we report a study of the structure of blends of PFO with a non-fluorescent polymer, namely poly(methylmethacrylate) (PMMA). If these two polymers are dissolved in a common solvent and then spin-coated, phase separation occurs due to the low entropy of mixing. The importance of studying polymer blends comes from the fact that many of the most efficient OLEDs and organic photovoltaic devices use blends of different conjugated polymers (Halls *et al.*, 2000).

Correspondence to: J. Chappell. E-mail: John.Chappell@sheffield.ac.uk

This allows composite material systems to be realized having high mobilities for both electrons and holes. This is important in OLED devices, as the efficient generation of electroluminescence requires balanced electron and hole currents. Although PMMA would not be employed as a charge transporting layer in an optoelectronic device (as it is highly insulating), a blend of PFO and PMMA provides an interesting system for study, as there is a complete absence of mixing between the materials. In addition, neutron reflectivity measurements indicate that the interfaces between PMMA and PFO are extremely sharp (around 2 nm). For these reasons PFO/PMMA blends present a useful system on which to test the optical resolution of a UV fluorescence NSOM. As we show below, phase separation between the PFO and PMMA occurs over a hierarchy of length-scales, with the smallest polymer domains detected being phase-separated regions of 250 nm in diameter. In some cases, the optical resolution of the fluorescence image is partly limited by large topographic variations in the surface of the film. Understanding the optical properties of relatively simple systems is important before examining more complex systems based on blends of different conjugated polymers. In conjugated-polymer blends, the distribution of fluorescence is often not well correlated with the blend morphology (Stevenson, 2001a,b) as efficient exciton-transfer occurs between the different components in the blend (even at low blend mixing ratios).

Figure 1 shows the absorption, photoluminescence and chemical structure of PFO. As can be seen, the absorption of PFO peaks in the near UV (at 370 nm), and emits blue fluorescence, which peaks (in the blue region of the spectrum) at 430 nm. PMMA in contrast is optically transparent at wavelengths down to ~250 nm and is non-fluorescent. We have studied PFO/PMMA blends at concentrations of 1%, 10% and 50% by weight of PFO in PMMA. The PFO and PMMA used had molecular weights of 388 kDa and 138 kDa, respectively. Solutions of the two materials were prepared by dissolving both polymers in toluene to a final concentration of 1% by mass. The solutions were then spin-coated onto quartz substrates, producing films with thickness between 40 nm and 250 nm. The film thickness was controlled by varying the coater spin speed. Film thickness was measured with a Dektak3 surface profilometer (Dektak, Veeco Instruments Ltd, Cambridge, U.K.).

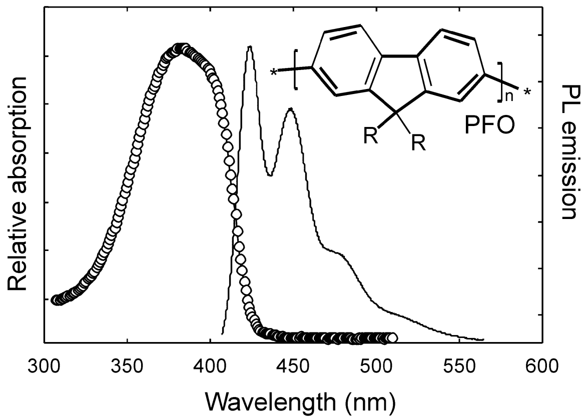

Fig. 1. The absorption (○) and photoluminescence (solid line) of PFO. The inset shows the chemical structure of PFO, where R = C_8H_{17}.

The films were characterized using a Topometrix Aurora NSOM (Veeco Instruments Ltd, Cambridge, U.K.), operating in transmission mode. Tip–sample distance was controlled by shear-force feedback with the probe mounted on a quartz crystal tuning fork. The NSOM probes used in our system were purchased commercially from Jasco International Ltd (Tokyo, Japan). These probes are fabricated by chemical etching and have a large cone-angle with an aperture that is determined by SEM to be between 60 and 80 nm in diameter. The large cone angle ensures that the probes have a high optical throughput (Suh & Zenobi, 2000), which is around 1.5% over the whole of the visible spectrum (including at 362 nm – the wavelength we use in these experiments). The probes also have negligible inherent fluorescence, making them ideal for sensitive NSOM spectroscopy of UV-absorbing materials. The excitation of the blend films was made through the NSOM tip using the 362 nm line from an argon-ion laser. The laser was first spectrally filtered using an interference filter to remove the laser plasma lines. This wavelength is very close to the peak of the PFO absorption, ensuring efficient generation of fluorescence. A 0.25 NA microscope objective positioned under the sample collected the PFO fluorescence and imaged it onto a photomultiplier photo-cathode. A UV rejection filter (OD 4) was placed in front of the PMT to remove the excitation light. Control experiments demonstrated that the optical signal detected by the photomultiplier originated from PFO fluorescence. The laser power focused into the NSOM fibre was approximately 0.4 mW. At this power we did not measure significant photo-induced degradation of the PFO over the course of the experiment. All imaging was done at room temperature and in air.

Figure. 2(a) and (b) show the topographic and NSOM images, respectively, of a 40 nm thick film of a blend of 50% PFO in PMMA. As it can be seen, the raised areas in the topographic image correspond closely to regions of low fluorescence emission. This allows us to identify the 'islands' as being PMMA, being surrounded by a PFO 'matrix'. Such structures are typical of phase separation in thin films based on a binary mix of polymers. Phase separation occurs during the later stages of the spin-coating process, as the evaporation of the solvent results in a rapid quench of the polymer blend which 'freezes-in' a non-equilibrium phase-separated morphology. The PMMA regions are frequently oblate, indicating that the film was subjected to significant shear-forces during spin-casting. The PMMA domains are estimated to have an average effective diameter of 1–2 μm. Within the PFO matrix, there are also a large number of much smaller domains, having an average diameter of 300 nm.

We measured a very similar surface structure using a Digital Instruments AFM (Veeco Instruments Ltd, Cambridge, U.K.),

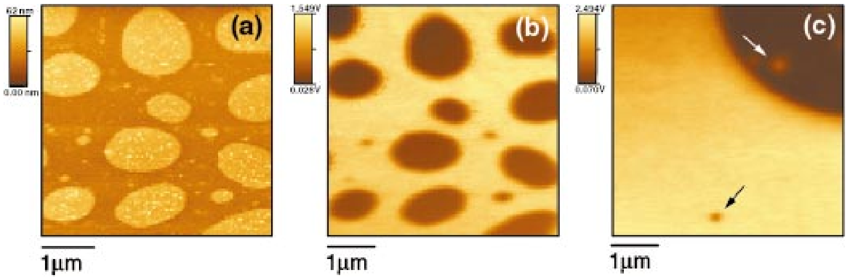

Fig. 2. (a) Topographic and (b) fluorescence images of a 50% PFO in PMMA 40 nm film; (c) fluorescence image from a 80 nm film of a 50% PFO in PMMA film. The white arrow indicates a trapped region of PFO in PMMA and the black arrow shows a region of PMMA in the PFO phase. The average dark-count (c) appears to be much larger than the average signal level recorded in (a) and (b). This increase in dark count probably originates from light escaping through a pinhole in the sidewall of the NSOM tip used to take this particular image. This leakage caused background fluorescence to be emitted from the PFO, resulting in an increase in the apparent background level. This background signal does not, however, appear to reduce the effective resolution of the image.

indicating that the NSOM tip is following the surface topography faithfully. The 300 nm diameter domains are characterized by an average height above the PFO phase of between 25 and 80 nm. Teetsov & Vanden Bout (2000) have identified domains of aggregated polymer in thin films of pure PFO which have solubilizing side-groups consisting of two hexyl-groups. It was shown that these aggregated regions (of diameter 50–150 nm) are less fluorescent (by about 20%) compared to the surrounding unaggregated PFO 'matrix'. It was also shown that such aggregated domains were largely absent in PFO having dodecyl side-groups. Our high resolution AFM scans (Ariu *et al.*, 2001) of pure films of poly(9,9-dioctylfluorene) (the material we use in this study) identify a very small number of aggregated regions: we typically find 10 or fewer such domains in a 5 μm^2 scan, each having a diameter of around 100 nm and height of 2–3 nm. Such a result is consistent with the fact that the longer octyl-side groups of poly(9,9-dioctylfluorene) improve the solubility of the polymer and thus significantly reduce aggregation. We thus conclude that the 300 nm diameter domains observed in a 50% blend of PFO in PMMA are composed of PMMA rather than aggregated PFO.

This conclusion is confirmed by the fact that both the 300 nm and the 1–2 μm domains are (within the dark-count of the detector) completely non-emissive. We thus conclude that there is no PFO layer located underneath the PMMA. This can be seen in the NSOM image of an 80 nm thick 50/50 blend film in Fig. 2(c). Here, we identify one such 300 nm diameter PMMA domain by a black arrow. It can also be seen that there are also small (300 nm diameter) PFO domains trapped within the 5 μm diameter PMMA domain (white arrow, Fig. 2c). As we will demonstrate below, such PFO domains are located at the surface of the PMMA phase. We can further confirm that these domains are composed almost entirely of PMMA. Using a Renishaw Raman microscope (Renishaw Plc, Wootton-under-Edge, Gloucestershire, U.K.), we have mapped the chemical composition of 50% PFO/PMMA blends. Measurements were made using the 633 nm line of a HeNe laser. Figures 3(a) and (b), respectively, show a white light image of a blend film together with a map of the characteristic (Ariu, 2001) (1600 cm^{-1}) Raman line of PFO (see the PFO Raman spectrum shown in Fig. 3c). This highly sensitive chemically-specific technique confirms that there is little or no PFO trapped below the PMMA-rich domains.

It is also apparent that as the average film thickness is increased from 40 nm to 80 nm, the average size of the large PMMA domains increases from 1 to 2 μm to around 5 μm. This indicates that the phase separation is influenced by dynamic processes that occur during spin-coating. This is because the speed at which the film is spun effectively changes the time over which the solvent is removed from the film and thus how fast the system is quenched. Similar observations have been reported on phase-separated thin-films of polystyrene and PMMA (Dalnoki-Veress *et al.*, 1997).

Figure. 4(a) and (b), respectively, show the topography and fluorescence emission for an 80 nm thick film of a 10% blend of PFO in PMMA. It can be seen that the minority phase (the PFO) now forms roughly circular domains in a PMMA matrix. These domains are between a few hundred nanometres and 1.5 μm in diameter and have an average depth of 30 nm below the surface of the PMMA phase. Preliminary analysis of both images indicate that these depressions constitute approximately 30% of the surface area of the film. As the blend contains 10% PFO by mass, we propose that there is vertical segregation, with a thin layer of PFO located on top of the PMMA. This reduction in the effective total thickness of the PFO is consistent with the fact that the intensity of fluorescence recorded from the 10% (and 1%) blend films is significantly smaller than that observed when recording the images presented in Fig. 2(b) and (c). It can be seen that there is a slight double tip artefact in the shear-force image, with the left-hand edges of the PFO domains appearing twice. We find that such effects can be problematic when using such chemically etched probes having a large taper angle on highly corrugated surfaces. This artefact does not, however, appear in the NSOM image.

We estimate the resolution of the optical image by identifying the smallest features that can be clearly resolved in both

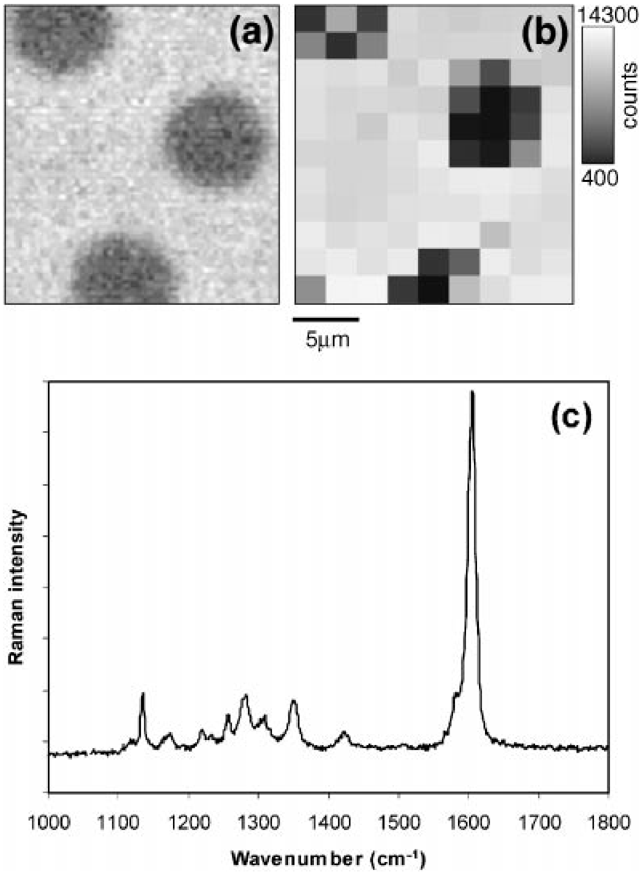

Fig. 3. (a) A white light image of a 50% blend film of PFO in PMMA. (b) Map of the Raman-scattered 1600 cm^{-1} line that is characteristic of a PFO phenyl-ring stretch mode. A Raman spectrum of PFO is shown in (c).

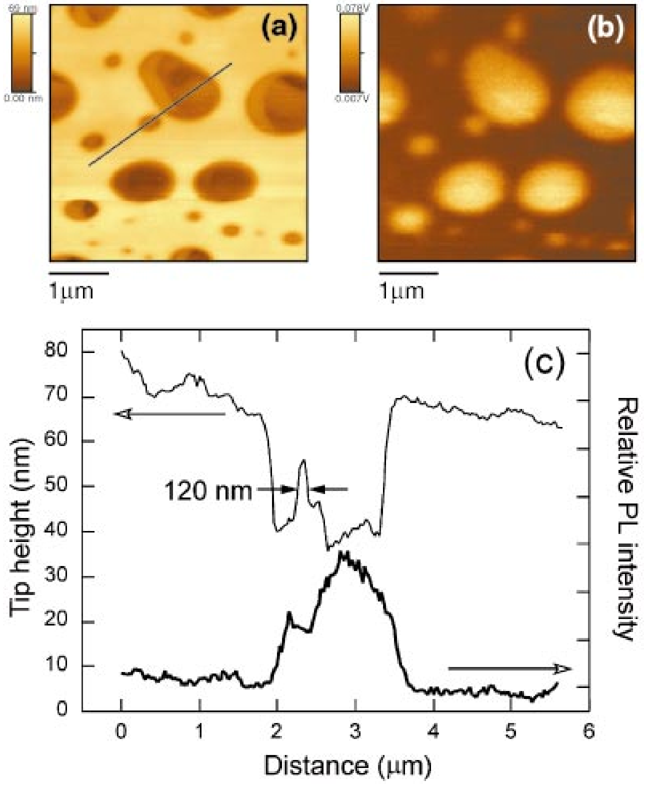

Fig. 4. (a, b) The topographic and fluorescence images, respectively, of a 40 nm film containing 10% PFO in PMMA; (c) a cross-section through both the topographic image and the NSOM image taken at the point indicated by the thick black line in (a).

the optical and shear force images. Figure 4(c) shows a cross-section of both the optical and topographic images taken along the line indicated in Fig. 4(a). It can be seen that there are two PMMA regions, separated by approximately 120 nm in the topographic image. These can just be resolved as being discreet domains in the NSOM image, and thus this represents the best resolution that we can achieve when imaging such films. To a good first approximation, the best optical resolution achievable using an NSOM tip is close to the size of the tip aperture (which in this case is between 60 and 80 nm). Thus, there are almost certainly a number of effects that contribute to our apparently reduced optical resolution. It is likely that in these blend films the resolution is partly limited by the film thickness. Even though the interface between the two polymers is very sharp, this boundary between the two layers is in fact a two-dimensional plane that lies normal to the substrate, buried beneath the film surface. We anticipate that by reducing the thickness of the film, it will be possible to improve the effective optical resolution, as the fluorescence generated will be closer to the optical near-field of the tip. We can estimate the range of distances over which fluorescence is generated: the extinction coefficient for light at 360 nm in PFO is 2.2×10^5 cm^{-1} (Ariu *et al.*, 2002), thus indicating that 10% of the laser flux is still able to generate fluorescence anywhere up to 100 nm from the film surface. Thus, reducing the film thickness well below the 40 nm thick films studied here may improve optical resolution. It is has been shown that changes in NSOM tip height also affects the resolution (Hecht *et al.*, 1997). The films studied here have very structured surfaces, having height changes of up to 70 nm, which again may well contribute to the image resolution.

Another important effect that contributes to NSOM resolution may originate from the fact that the PMMA is transparent to the excitation laser. Thus, when the tip is positioned above a PMMA region, fluorescence may still be generated from surrounding PFO regions as the laser light may propagate a significant distance within the PMMA. This effect is likely to be significant in the films whose topographic and NSOM images are shown in Fig. 5(a) and (b), respectively. These images were recorded for a 250 nm thick film of a 1% blend of PFO in PMMA. The NSOM image is characterized by a large number of small emissive domains of diameter between 250 and 450 nm. These emissive regions correlate with 10 nm deep depressions in film surface. Analysis of the topographic image

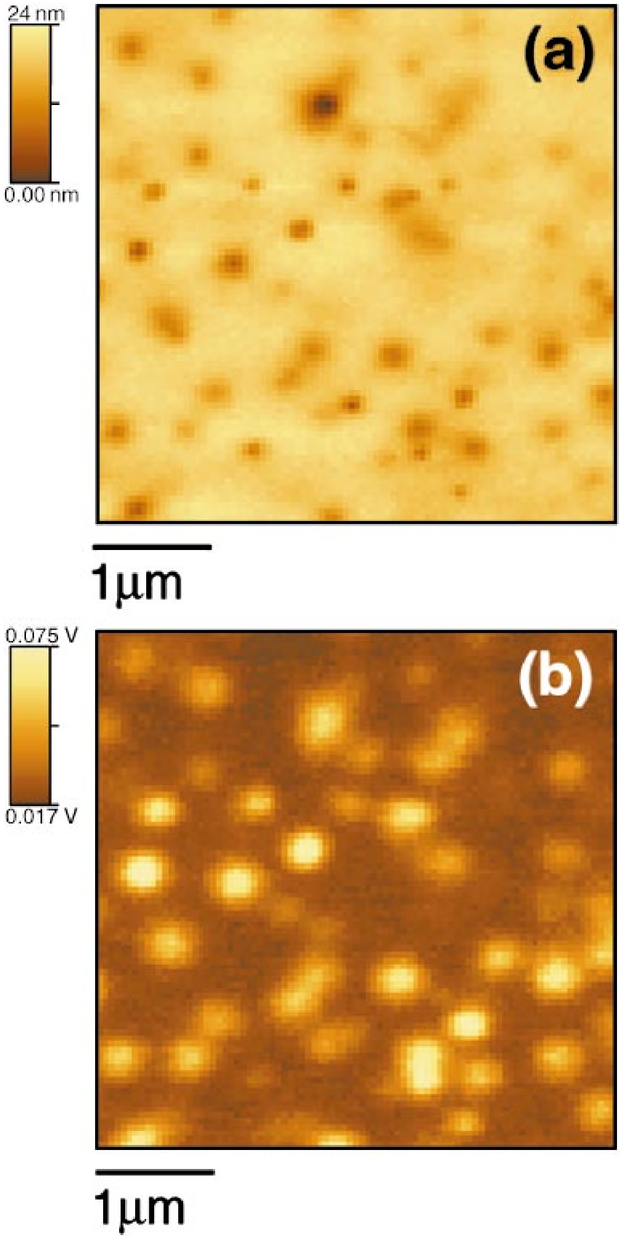

Fig. 5. (a, b) The topographic and fluorescence images, respectively, of a 250 nm film containing 1% PFO in PMMA.

indicates that these depressions constitute approximately 10% of the surface area of the film. As the blend contains 1% PFO by mass, it again appears that as was observed in the blend films containing 10% PFO, there is vertical segregation, with a thin layer (estimated to be a few nanometres thick) of PFO located on top of the PMMA. Interestingly, we find that there is a wide range in the fluorescence intensity from each of these PFO domains, indicating that there is a significant variation in the local thickness of the PFO located at the surface of the PMMA. The fact that PFO preferentially lies on top of the PMMA is in agreement with other studies (Higgins *et al.*, submitted), which indicate that bilayer films of PMMA deposited on top of PFO become unstable and de-wet when raised to temperatures in excess of 160 °C.

It is clear that the optical resolution of the NSOM image is not significantly better than that observed in thicker 50% blend films, even though the PFO film is much thinner. Here, the propagation of the UV excitation light in the thick underlying PMMA matrix is likely to be significant. It is also clear that even though the interface between the PFO and PMMA is very sharp, the lateral (x,y) interface between the different PFO phase-separated regions at the surface may be much less well defined. The topographic image confirms that the depressions that correlate with the fluorescence are not particularly well delineated, indicating that there may at some points be a very thin, almost continuous layer of PFO connecting the different phase-separated domains.

We have thus observed a hierarchy of phase separation in the blend films, which we show can be controlled by varying the film thickness. We identify both PMMA and PFO domains having length scales down to 250 nm. Such positive identification could not easily be achieved using a far-field microscope. Only by comparing the NSOM image with the shear-force image can a complete determination of the whole film structure be made. Our work further demonstrates the ability of NSOM to perform detailed imaging and characterization of complex disordered organic thin films.

Acknowledgements

J.C. and D.G.L. thank the U.K. EPSRC for a Studentship and an Advanced Research Fellowship, respectively, and for support via grants GR/R26658/01 and GR/R10479/01. We also thank Drs M. Bernius and R. B. Fletcher at the Dow Chemical Company (U.S.A.) for the polyfluorene used in this work.

References

Ariu, M., Lidzey, D.G., Lavrentiev, M., Bradley, D.D.C., Jandke, M. & Strohriegl, P. (2001) A study of the different structural phases of the polymer poly(9,9-dioctylfluorene) using Raman spectroscopy. *Synthetic Metals*, **116**, 217–221.

Ariu, M., Lidzey, D.G., Sims, M., Cadby, A.J., Lane, P.A. & Bradley, D.D.C. (2002) The effect of morphology on the temperature-dependent photoluminescence quantum efficiency of the conjugated polymer poly(9,9-dioctylfluorene). *J. Physics – Condensed matter*, **14**, 9975–9986, OCT 28.

Dalnoki-Veress K., Forrest, J.A., Stevens, J.R. & Dutcher, J.R. (1997) Phase separation morphology of spin-coated polymer blend thin films. *Physica A*, **239**, 87–94.

DeAro, J.A., Weston, K.D., Buratto, S.K. & Lemmer, U. (1997) Mesoscale optical properties of conjugated polymers probed by near-field scanning optical microscopy. *Chem. Physics Lett.* **277**, 532–538.

DeAro, J.A. & Buratto, S.K. (1999) Near-field photoconductivity of stretch-oriented poly(para-phenylene vinylene). *Appl. Phys. Lett.* **75**, 3814–3816.

Grell, M., Bradley, D.D.C., Ungar, G., Hill, J. & Whitehead, K.S. (1999) Interplay of physical structure and photophysics for a liquid crystalline polyfluorene. *Macromolecules*, **32**, 5810–5817.

Grice, A.W., Bradley, D.D.C., Bernius, M.T., Inbasekaran, M., Wu, W.W. & Woo, E.P. (1998) High brightness and efficiency blue light-emitting polymer diodes. *Appl. Phys. Lett.* **73**, 629–631.

Halls, J.J.M., Arias, A.C., MacKenzie, J.D., Wu, W.S., Inbasekaran, M., Woo, E.P. & Friend, R.H. (2000) Photodiodes based on polyfluorene composites: Influence of morphology. *Adv. Mater.* **12**, 498–502.

Hecht, B., Bielefeldt, H., Inouye, Y., Pohl, D.W. & Novotny, L. (1997) Facts and artifacts in near-field optical microscopy. *J. Appl. Phys.* **81**, 2492–2498.

Higgins, A.M., Jukes, P.C., Martin, S.J., Geoghegan, M., Jons, R.A.L. & Cubitt, R. (2002) A neutron reftectometry study of the interface between poly(9,9-dioctylfluorene) and poly(methyl methacrylate). *Appl. Phys. Lett.* **81**, 4949.

Hsu, J.H., Wei, P.K., Fann, W.S., Chuang, K.R. & Chen, S.A. (1998) The inhomogeneity in conjugated polymer blend films. *Ultramicroscopy*, **71**, 263–267.

Kwak, E.S., Kang, T.J. & Vanden Bout, D.A. (2001) Fluorescence lifetime imaging with near-field scanning optical microscopy. *Anal. Chem.* **73**, 3257–3262.

Nabetani, Y., Yamasaki, M., Miura, A. & Tamai, N. (2001) Fluorescence dynamics and morphology of electroluminescent polymer in small domains by time-resolved SNOM. *Thin Solid Films*, **393**, 329–333.

Paesler, M.A. & Moyer, P.J. (1996) *Near Field Optics*. Wiley, New York.

Redecker, M., Bradley, D.D.C., Inbasekaran, M. & Woo, E.P. (1999) Mobility enhancement through homogeneous nematic alignment of a liquid-crystalline polyfluorene. *Appl. Phys. Lett.* **74**, 1400–1402.

Stevenson, R., Granström, M. & Richards, D. (1999) Fluorescence scanning near-field optical microscopy of conjugated polymer blends. *Appl. Phys. Lett.* **75**, 1574–1576.

Stevenson, R., Milner, R.G., Richards, D., Arias, A.C., Mackenzie, J.D., Halls, J.J.M., Friend, R.H., Kang, D.-J. & Blamire, M. (2001a) Fluorescence scanning near-field optical microscopy of polyfluorene composites. *J. Microsc.* **202**, 433–438.

Stevenson, R., Riehn, R., Milner, R.G., Richards, D., Moons, E., Kang, D.-J., Blamire, M., Morgado, J. & Cacialli, F. (2001b) Ultraviolet-visible near-field microscopy of phase-separated blends of polyfluorene-based conjugated semiconductors. *Appl. Phys. Lett.* **79**, 833–835.

Suh, Y.D. & Zenobi, R. (2000) Improved probes for scanning near-field optical microscopy. *Adv. Mater.* **12**, 1139–1142.

Teetsov, J. & Vanden Bout, D.A. (2000) Near-field scanning optical microscopy (NSOM) studies of nanoscale polymer ordering in pristine films of poly(9,9-dialkylfluorene). *J. Phys. Chem. B*, **104**, 9378–9387.

Teetsov, J. & Vanden Bout, D.A. (2002) Near-field scanning optical microscopy studies of nanoscale order in thermally annealed films of poly(9,9-diakylfluorene). *Langmuir*, **18**, 897–903.

Virgili, T., Lidzey, D.G. & Bradley, D.D.C. (2000) Efficient energy transfer from blue to red in tetraphenylporphyrin-doped poly(9,9-dioctylfluorene) light emitting diodes. *Adv. Mater.* **12**, 58–62.

Webster, X., Smith, D.A., Batchelder, D.N., Lidzey, D.G. & Bradley, D.D.C. (1998) Application of fluorescence scanning near-field optical microscopy to the study of phase-separated conjugated polymers. *Ultramicroscopy*, **71**, 275–279.